Tuyển tập Hội nghị khoa học toàn quốc lần thứ nhất về Động lực học và Điều khiển
Đà Nẵng, ngày 19-20/7/2019, tr. 222-229, DOI 10.15625/vap.2019000282

On the Lengths of Driving Cables in a Spatial Multi-Section Continuum Robot

Duong Xuan Bien, Chu Anh My, Nguyen Van Cong, Do Tien Lap
Le Quy Don Technical University,
No. 236, Hoang Quoc Viet Street, Cau Giay District, Vietnam
E-mail: xuanbien82@yahoo.com

Abstract

In this article, a spatial multi-section continuum robot with elastic backbone is considered. The movement of backbone is driven by cable wires through the main. The kinematic characteristics of the continuum robot are demonstrated by modeling the kinematics of its flexible backbone. The relationship between the joint variables in joint space and the position variables in workspace is shown by building the kinematic equations based on some specific assumptions. The lengths of driving cables of each section are calculated based on the results of the inverse kinematics problem. The geometries of support disks are considered while calculating the lengths of driving cables. The results of this research can be used to design the control system.

Keywords: Kinematic modeling, continuum robots, cables-driven length, inverse kinematics

1. Introduction

In the field of robotics, because of their dexterity, continuum robots become increasingly popular and is found in a wide range of applications such as minimally invasive surgery, escape works, pipeline engineering and military. Continuum robots are designed based on mimicking locomotion mechanisms of soft bodies existing in the nature such as octopus [1], [2], [3], [4], [5], snake [6], and trunk of elephant [2]. Continuum robots have great potential in medicine [7], [8]. There are two types of continuum robot structures which are focused in research: rigid structures and soft structures that are depending on the fabricated materials of each part of the robot. The first type is to use rigid parts connected together or have parallel structures [1], [9]. The second type of continuum robots uses an elastic backbone consisting of many circular sections. They are controlled by secondary backbones or cable wires [10], [11], [12], [13], or tendon [8], [14], [15], [16], [17]. This type of continuum robot is the subject of research in this paper.

The backbone is an elastic rod which is divided into many serial arcs called sections. All sections are characterized by parameters which are length of arc, curvature and bending angle. To reduce the complexity when analyzing kinematics, the value of the curvature is assumed constant along each arc [18]. The motion of continuum robots is executed by motors through the cables. The lengths of driving cables are calculated based on the variety of joint variables on each section and the geometries of support disks. The properties of continuum robots are examined where in the lengths of bending segments can be adjusted in [19]. The ability to various section lengths would allow continuum robots to assume a significantly wider range of configurations than in existing designs, expanding their potential range of applications. The kinematic modeling and the inverse kinematic problem for a spatial continuum robot first type are presented based on D-H techniques in [20]. Particle Swarm Optimization is used to find the optimal joint variables for the inverse kinematics of a two-section planar continuum robots in [21]. These authors then investigated model of parallel robots used for the computation of the link's length in [22] to solve inverse kinematics. The endpoint coordinates of each bending section are determined using a metaheuristic method. Authors in [23] introduced, described and tested a novel design of continuum robot which has a twin-pivot compliant joint construction that minimizes the twisting around its axis. A kinematics model is introduced which can be applied to a wide range of twin-pivot construction with two pairs of cables per section. According to this model, the approach for minimising the kinematic error is developed. The length of driving cables was considered. The inverse kinematics for a tendon-driven continuum robot is derived based on an developed open-loop controller and 3D joystick in [17]. The performance of the open-loop system was evaluated by drawing basic geometrical shapes and tracking recorded errors. A tendon-driven continuum robot with two joints and passive flexibility is presented in [24]. The inverse kinematic problem is solved based

on the protopyte physical structure and closed-loop controller. Authors in [9] presented a novel approaches of kinematic modeling of the wire-driven universal joint continuum robot which has variable backbone hardness. The kinematic and dynamic modeling of a planar driving cables single-section continuum robot is concerned in [13]. A comprehensive static model of driving cables multi-section continuum robot is investigated considering friction effect in [12]. The kinematics modeling of endoscopic robot is described based on Lie group theory [18].

In this paper, a spatial multi-section continuum robot is considered. The kinematics modeling of this robot is presented through building the kinematic equations of the backbone. The inverse kinematics problem of spatial three-section continuum robot is solved using closed-loop algorithm. The solutions of joint variables in inverse kinematics are the input data to calculate the lengths of driving cables of each section. The results of this research can be used to design the control system.

2. Kinematic modeling

Consider the three-section continuum robot in Fig. 1. Each section is driven by three cables. To reduce the complexity of the kinematic modeling, assume that the curvature is constant within each section.

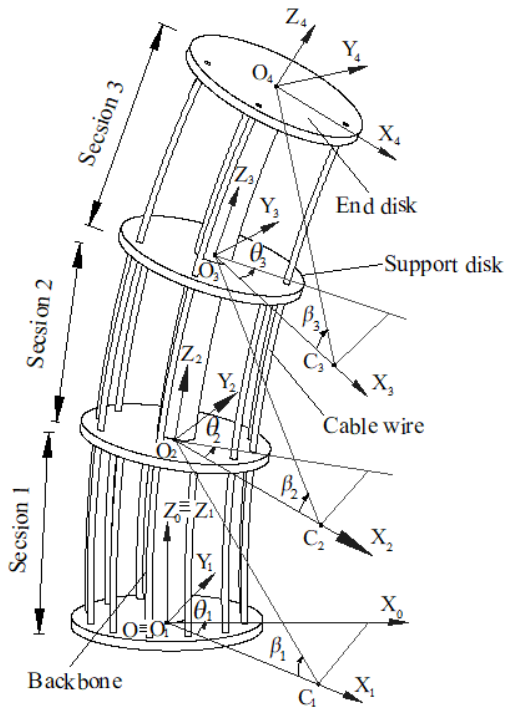

Figure 1. A spatial three-section continuum robot

Where, $(OXYZ)_0$ is the fixed coordinate system. The frames $(OXYZ)_i; i = 1,2,3$ are the local coordinate systems which are attached to the respective sections. The origin of local frame is always at the first point of each section. Each axis $(OZ)_i$ is tangent to the arc of each section at the origin of frame. C_i is the centre curvature of each arc section i. These centres are always on the local $(OX)_i$. The other axes are determined by the right-hand rule. Define some symbols for section i that:

The backbone length is L_{0i}, the curvature is κ_{0i}, the bending angle is β_i, the orientation angle is θ_i. The lengths of driving cables when $\beta_i = 0$ are L_{i1}, L_{i2} and L_{i3}. The radiuses of arcs are R_{i1}, R_{i2} and R_{i3}. The deviational lengths of driving cables are $\Delta L_{i1}, \Delta L_{i2}$ and ΔL_{i3}. The radius of circles through the center of holes which are used to thread the driving cables is r_i. The parameters of bending arc of section i are related to each other according to formula as below

$$\beta_i(t) = s_i(t)\kappa_i(t); i = 1,2,3 \quad (1)$$

Where $s_i(t)$ is the length of arc i. The position vector of the section 1 endpoint in the local frame $(OXYZ)_1$ is determined as

$$\mathbf{r}_1 = \left[\frac{1}{\kappa_1}(1-\cos\beta_1) \quad 0 \quad \frac{1}{\kappa_1}\sin\beta_1\right]^T \quad (2)$$

The position of this point in the fixed frame $(OXYZ)_0$

$$\mathbf{r}_{01} = \mathbf{T}_1\mathbf{r}_1 = \begin{bmatrix} \frac{1}{\kappa_1}(1-\cos\beta_1)\cos\theta_1 \\ \frac{1}{\kappa_1}(1-\cos\beta_1)\sin\theta_1 \\ \frac{1}{\kappa_1}\sin\beta_1 \end{bmatrix} \quad (3)$$

where $\mathbf{T}_1$ is the rotational matrix around $(OZ)_1$

$$\mathbf{T}_1 = \begin{bmatrix} \cos\theta_1 & -\sin\theta_1 & 0 \\ \sin\theta_1 & \cos\theta_1 & 0 \\ 0 & 0 & 1 \end{bmatrix} \quad (4)$$

Similarly, the position vector of endpoint of section 2 (O_3) in frame $(OXYZ)_2$ is calculated as

$$\mathbf{r}_2 = \begin{bmatrix} \frac{1}{\kappa_2}(1-\cos\beta_2) & 0 & \frac{1}{\kappa_2}\sin\beta_2 \end{bmatrix}^T \quad (5)$$

To determine the position vector of end-effector point of section 2 (O_3) in fixed frame $(OXYZ)_0$, the steps are executed as follow

- Rotate the frame $(OXYZ)_2$ around axis OZ_2 with angle θ_2, we have the rotational matrix

$$\mathbf{T}_2 = \begin{bmatrix} \cos\theta_2 & -\sin\theta_2 & 0 \\ \sin\theta_2 & \cos\theta_2 & 0 \\ 0 & 0 & 1 \end{bmatrix} \quad (6)$$

- Rotate the frame received around axis OY_1 with angle β_1, the rotational matrix is described as

$$\mathbf{T}_{1y} = \begin{bmatrix} \cos\beta_1 & 0 & \sin\beta_1 \\ 0 & 1 & 0 \\ -\sin\beta_1 & 0 & \cos\beta_1 \end{bmatrix} \quad (7)$$

- Rotate the new frame around axis OZ_1 with angle θ_1 following the matrix in (4).

The position vector of endpoint of section 2 in fixed frame is calculated as

$$\mathbf{r}_{02} = \mathbf{r}_{01} + \mathbf{T}_1\mathbf{T}_{1y}\mathbf{T}_2\mathbf{r}_2 \quad (8)$$

Similarly, the position vector of endpoint of section 3 in fixed frame is given as

$$\mathbf{r}_{03} = \mathbf{r}_{02} + \mathbf{T}_1\mathbf{T}_{1y}\mathbf{T}_2\mathbf{T}_{2y}\mathbf{T}_3\mathbf{r}_3 = \begin{bmatrix} xE & yE & zE \end{bmatrix}^T \quad (9)$$

Specific coordinates of the end-effector coordinates of a spatial three-section continuum robot in $(OXYZ)_0$ can be calculated by using MAPLE software as

$$xE := \frac{\cos(\theta 1)\,(1-\cos(\beta 1))}{k1} + \frac{(\cos(\theta 1)\cos(\beta 1)\cos(\theta 2) - \sin(\theta 1)\sin(\theta 2))\,(1-\cos(\beta 2))}{k2} + \frac{\cos(\theta 1)\sin(\beta 1)\sin(\beta 2)}{k2}$$
$$+ \frac{1}{k3}((((\cos(\theta 1)\cos(\beta 1)\cos(\theta 2) - \sin(\theta 1)\sin(\theta 2))\cos(\beta 2) - \cos(\theta 1)\sin(\beta 1)\sin(\beta 2))\cos(\theta 3) + (-\cos(\theta 1)\cos(\beta 1)\sin(\theta 2)$$
$$- \sin(\theta 1)\cos(\theta 2))\sin(\theta 3))\,(1-\cos(\beta 3))) + \frac{((\cos(\theta 1)\cos(\beta 1)\cos(\theta 2) - \sin(\theta 1)\sin(\theta 2))\sin(\beta 2) + \cos(\theta 1)\sin(\beta 1)\cos(\beta 2))\sin(\beta 3)}{k3}$$

$$yE := \frac{\sin(\theta 1)\,(1-\cos(\beta 1))}{k1} + \frac{(\sin(\theta 1)\cos(\beta 1)\cos(\theta 2) + \cos(\theta 1)\sin(\theta 2))\,(1-\cos(\beta 2))}{k2} + \frac{\sin(\theta 1)\sin(\beta 1)\sin(\beta 2)}{k2}$$
$$+ \frac{1}{k3}((((\sin(\theta 1)\cos(\beta 1)\cos(\theta 2) + \cos(\theta 1)\sin(\theta 2))\cos(\beta 2) - \sin(\theta 1)\sin(\beta 1)\sin(\beta 2))\cos(\theta 3) + (-\sin(\theta 1)\cos(\beta 1)\sin(\theta 2)$$
$$+ \cos(\theta 1)\cos(\theta 2))\sin(\theta 3))\,(1-\cos(\beta 3))) + \frac{((\sin(\theta 1)\cos(\beta 1)\cos(\theta 2) + \cos(\theta 1)\sin(\theta 2))\sin(\beta 2) + \sin(\theta 1)\sin(\beta 1)\cos(\beta 2))\sin(\beta 3)}{k3} \quad (10)$$

$$zE := \frac{\sin(\beta 1)}{k1} - \frac{\sin(\beta 1)\cos(\theta 2)\,(1-\cos(\beta 2))}{k2} + \frac{\cos(\beta 1)\sin(\beta 2)}{k2} + \frac{(-\sin(\beta 1)\cos(\theta 2)\sin(\beta 2) + \cos(\beta 1)\cos(\beta 2))\sin(\beta 3)}{k3}$$
$$+ \frac{((-\sin(\beta 1)\cos(\theta 2)\cos(\beta 2) - \cos(\beta 1)\sin(\beta 2))\cos(\theta 3) + \sin(\beta 1)\sin(\theta 2)\sin(\theta 3))\,(1-\cos(\beta 3))}{k3}$$

We can generalize for the spatial n-section continuum robot, the position vector of end-effector in $(OXYZ)_0$ is given as

$$\mathbf{r}_{0E} = \mathbf{r}_{0(n-1)} + \mathbf{T}_1\mathbf{T}_{1y}\mathbf{T}_2 \ldots \mathbf{T}_{n-1}\mathbf{T}_{(n-1)y}\mathbf{T}_n\mathbf{r}_{nE} \quad (11)$$

3. Inverse kinematics and the changes in the lengths of driving cables

3.1. Inverse kinematics analyzing

Assume that the path $\mathbf{x}_d(t), \dot{\mathbf{x}}_d(t)$ in workspace is given. The goal is to find the joint variables in joint space $\mathbf{q}(t), \dot{\mathbf{q}}(t)$ that reproduce the given path. Define

the joint variable vector for a n -section spatial continuum robot as

$$\mathbf{q}(t) = \begin{bmatrix} \mathbf{q}_1^T & \mathbf{q}_2^T & \dots & \mathbf{q}_n^T \end{bmatrix}^T \quad (12)$$

where, $\mathbf{q}_i = \begin{bmatrix} \kappa_i & \beta_i & \theta_i \end{bmatrix}; i = 1 \div n$ is the joint variables vector of section i.

The forward kinematic equations can be given as

$$\mathbf{x} = f(\mathbf{q}) \quad (13)$$

The differential kinematics equation is described as

$$\dot{\mathbf{x}} = \mathbf{J}(\mathbf{q})\dot{\mathbf{q}} \quad (14)$$

The Jacobian matrix $\mathbf{J}(\mathbf{q})$ with size $3 \times 3n$. The multi-section spatial continuum robot is the redundant system. The inverse kinematic problem for a redundant robot has multiple solutions in general. Due to the non-square Jacobian matrix for $3n$ DOFs robot, the basic inverse solution to (15) is obtained by using the pseudoinverse $\mathbf{J}^*$ of the matrix $\mathbf{J}$ and the inverse solution can then be written as

$$\dot{\mathbf{q}} = \mathbf{J}^*(\mathbf{q})\dot{\mathbf{x}} \quad (15)$$

where, the pseudoinverse $\mathbf{J}^*$ can be computed as in [7].

Open-loop solutions of joint variables through numerical integration unavoidably lead to errors in workspace. In order to overcome these drawbacks, the closed-loop algorithm is used based on the path error $\mathbf{e}$ in workspace between the desired and actual path. Consider the location error $\mathbf{e}$ and its derivative $\dot{\mathbf{e}}$ which can be given as

$$\mathbf{e} = \mathbf{x}_d - \mathbf{x}; \dot{\mathbf{e}} = \dot{\mathbf{x}}_d - \dot{\mathbf{x}} \quad (16)$$

The inverse kinematic solution of redundant robot based on closed-loop algorithm is given as [8]

$$\dot{\mathbf{q}} = \mathbf{J}^*(\mathbf{q})(\dot{\mathbf{x}}_d + \mathbf{K}_p(\mathbf{x}_d - \mathbf{x})) + (\mathbf{I} - \mathbf{J}^*(\mathbf{q})\mathbf{J}(\mathbf{q}))\dot{\mathbf{q}}_0 \quad (17)$$

Where, $\mathbf{K}_p$ is a symmetric positive definite matrix.

3.2. Calculate the lengths of driving cables

Consider the cable wires of section 1 in Fig 2. The deviation of length of the first driving cable can be calculated as

$$\Delta L_{11} = L_{01} - L_{11} = (R_{01} - R_{11})\beta_1 = \beta_1 r_1 \cos\theta_1 \quad (18)$$

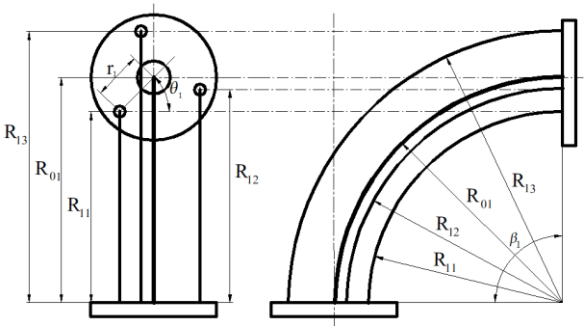

Figure 2 . The section 1 in $(\mathrm{OXZ})_1$

Assume that the angle between the holes is $\frac{2\pi}{3}$. The deviation of lengths of all driving cables of section 1 given as

$$\begin{aligned} \Delta L_{11} &= r_1\beta_1 \cos\theta_1 \\ \Delta L_{12} &= r_1\beta_1 \cos(\theta_1 - \frac{2\pi}{3}) \\ \Delta L_{13} &= r_1\beta_1 \cos(\theta_1 + \frac{2\pi}{3}) \end{aligned} \quad (19)$$

When the section 1 moves, the deviation of lengths of three cables of section 2 is determined as

$$\begin{aligned} \Delta L'_{21} &= r_2\beta_1 \cos\theta_1 \\ \Delta L'_{22} &= r_2\beta_1 \cos(\theta_1 - \frac{2\pi}{3}) \\ \Delta L'_{23} &= r_2\beta_1 \cos(\theta_1 + \frac{2\pi}{3}) \end{aligned} \quad (20)$$

When the both section 1 and section 2 are driven, the deviation of lengths of three cables of section 2 can be calculated as

$$\begin{aligned} \Delta L_{21} &= r_2\beta_1 \cos\theta_1 + r_2\beta_2 \cos\theta_2 \\ \Delta L_{22} &= r_2\beta_1 \cos(\theta_1 - \frac{2\pi}{3}) + r_2\beta_2 \cos(\theta_2 - \frac{2\pi}{3}) \\ \Delta L_{23} &= r_2\beta_1 \cos(\theta_1 + \frac{2\pi}{3}) + r_2\beta_2 \cos(\theta_2 + \frac{2\pi}{3}) \end{aligned} \quad (21)$$

Similarly, when all of sections are driven, the deviation of lengths of driving cables of section 3 are given as

$$\begin{aligned} \Delta L_{31} &= r_3\beta_1 \cos\theta_1 + r_3\beta_2 \cos\theta_2 + r_3\beta_3 \cos\theta_3 \\ \Delta L_{32} &= r_3\beta_1 \cos(\theta_1 - \frac{2\pi}{3}) + r_3\beta_2 \cos(\theta_2 - \frac{2\pi}{3}) + r_3\beta_3 \cos(\theta_3 - \frac{2\pi}{3}) \\ \Delta L_{33} &= r_3\beta_1 \cos(\theta_1 + \frac{2\pi}{3}) + r_3\beta_2 \cos(\theta_2 + \frac{2\pi}{3}) + r_3\beta_3 \cos(\theta_3 + \frac{2\pi}{3}) \end{aligned} \quad (22)$$

Expanding with n sections, the deviation of lengths of driving cables of section n can be shown as

$$\begin{aligned}
\Delta L_{n1} &= r_n\beta_1\cos\theta_1 + r_n\beta_2\cos\theta_2 + ... + r_n\beta_n\cos\theta_n \\
\Delta L_{n2} &= r_n\beta_1\cos(\theta_1 - \frac{2\pi}{3}) + r_n\beta_2\cos(\theta_2 - \frac{2\pi}{3}) + ... + r_n\beta_n\cos(\theta_n - \frac{2\pi}{3}) \\
\Delta L_{n3} &= r_n\beta_1\cos(\theta_1 + \frac{2\pi}{3}) + r_n\beta_2\cos(\theta_2 + \frac{2\pi}{3}) + ... + r_n\beta_n\cos(\theta_n + \frac{2\pi}{3})
\end{aligned} \tag{23}$$

Fig. 3 describes the geometries of constant support disks for three sections. Each section has three driving cables. So, the support disks of section 1 have nine holes which are evenly distributed on a circle with $r_1 = r_2 = r_3$. Fig. 4 shows support disks which have the varied cross-section. The nine holes on disks of section 1 are distributed on three different circles which have the radius r_1, r_2, r_3.

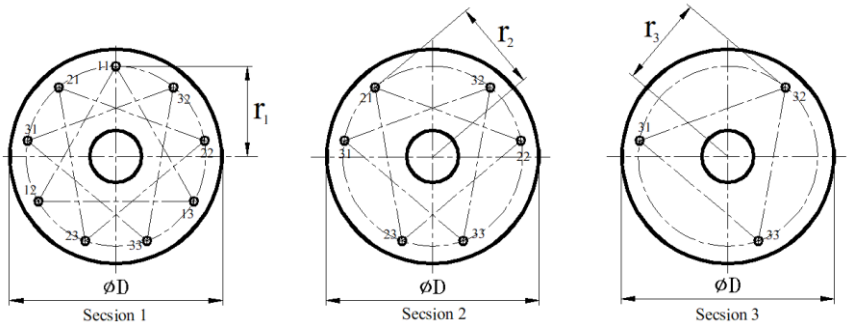

Figure 3. The constant end disk structure of three sections

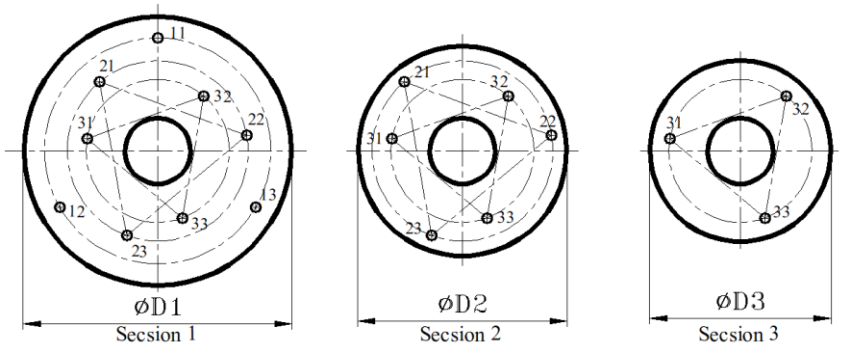

Figure 4. The varied end disk structure of three sections

3.3. Numerical simulation

Apply the inverse kinematic algorithm for a spatial three-section continuum robot with the desired path as

$$\begin{cases} x_E = 0.6 + 0.2\sin(t) \quad (m) \\ y_E = 0.1 + 0.5\cos(t) \quad (m) \\ z_E = 0.4 - 0.1\cos(t) \quad (m) \end{cases} \tag{24}$$

The backbone lengths of three sections are $L_{01} = 0.3(m); L_{02} = 0.5(m)$ and $L_{03} = 0.7(m)$. The radius of circles are $r_1 = r_2 = r_3 = 10(mm)$. Fig. 5 shows the diagram to solve the inverse kinematics and calculate the length of driving cables of sections in SIMULINK.

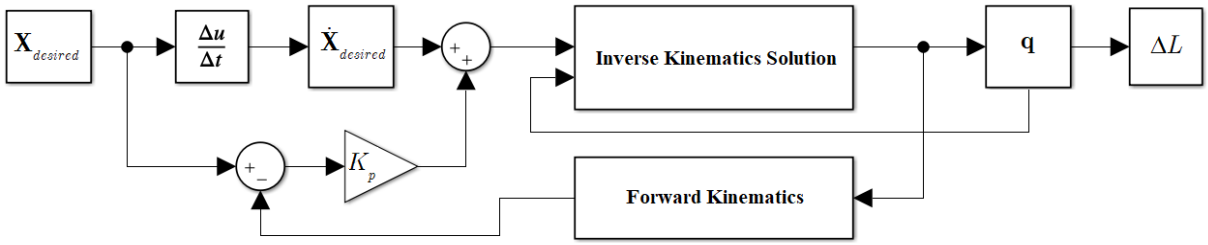

Figure 5. The calculated diagram of the inverse kinematics and the length of driving cables in SIMULINK

The desired position and velocity of end-effector are shown as Fig. 6 and Fig. 7. The simulation results are described from Fig. 8 to Fig. 11. Fig. 8 shows the curvatures of sections. The maximum curvature of sections are $2.25(m^{-1})$, $2(m^{-1})$ and $1.5(m^{-1})$. The large the curvature value, the smaller the radius of arc value. Fig. 9 describes the bending angles in the bending planes OXZ. The maximum bending angle of sections are $0.4(rad), 1.7(rad)$ and $0.25(rad)$. The orientation angles of sections are shown in Fig. 10. The location errors values of end-effector on axes $(OX)_0, (\mathrm{OY})_0$ and $(OZ)_0$ are presented in Fig. 11.

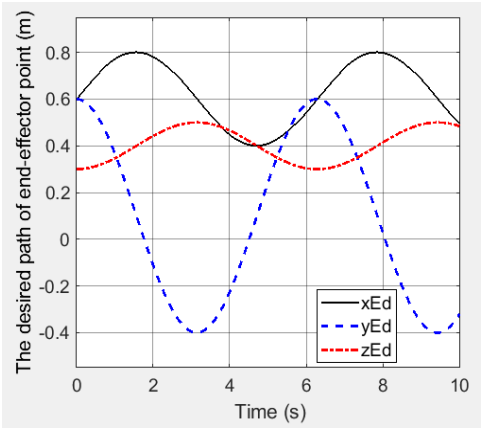

Figure 6. The desired endpoint path in the workspace

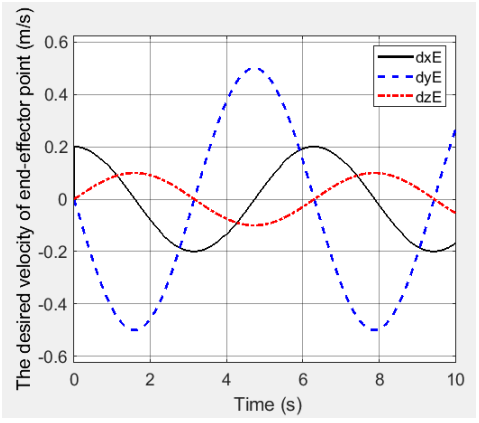

Figure 7. The desired endpoint velocity in the workspace

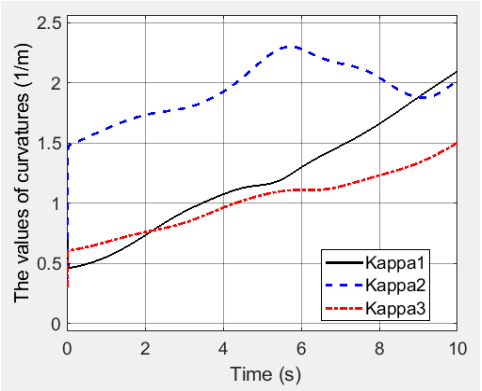

Figure 8. The curvature values of three sections

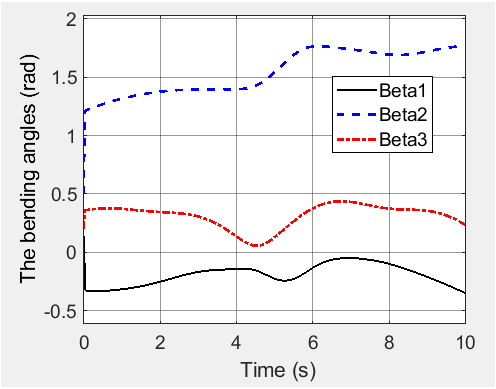

Figure 9. The bending angle values of three sections

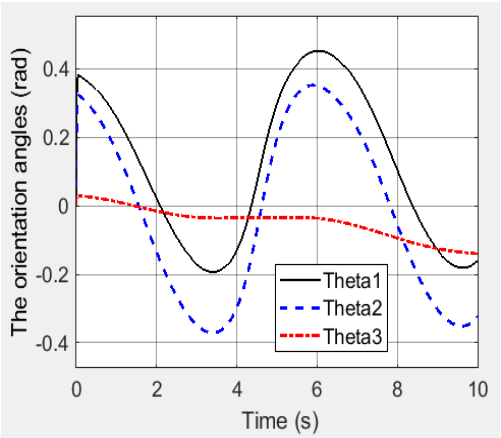

Figure 10. The orientation angle values of three sections

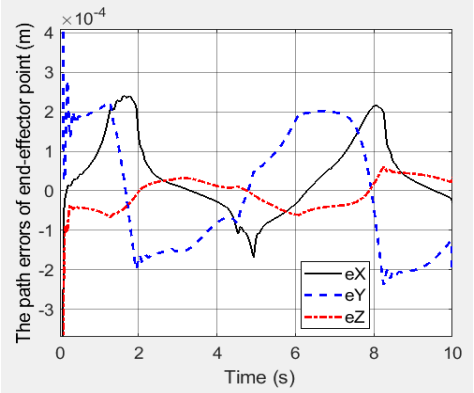

Figure 11. The path error of endpoint in workspace

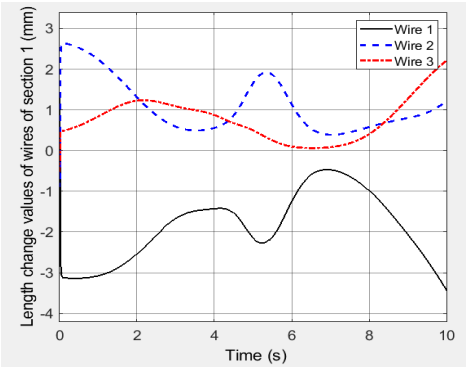

Figure 12. The deviation of lengths of driving cables of first section

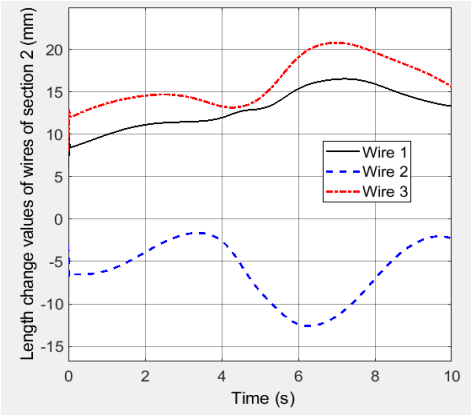

Figure 13. The deviation of lengths of driving cables of second section

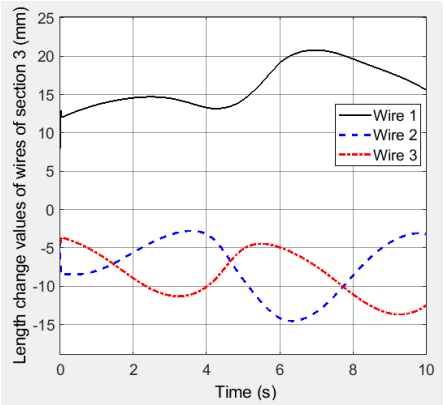

Figure 14. The deviation of lengths of driving cables of third section

Fig. 12, Fig. 13 and Fig. 14 show the length of each driving cables on sections. In the Fig. 12, the cable 1 of section 1 has the maximum length change with $3.5(mm)$.

Fig. 13 shows that, the cable 3 of section 2 has the maximum length change with $21(mm)$. Similarly, the cable 1 of section 3 has the maximum value with $22(mm)$.

4. Conclusion

Continuum robots commonly do not contain any actuators in the robot structure itself, making them relatively compact and lighweight. Opposite, the motion transfer problem for continuum robots is becoming a challenge. In this paper, a spatial three-section continuum robot is mentioned. The motion of continuum robots is executed by motors through the driving cables. The lengths of driving cables are calculated based on the variety of joint variables on each section and the geometries of support disks. Simulation results have important meaning in designing the control system and selection the actuators.

Acknowledgements

This research is funded by Vietnam National Foundation for Science and Technology Development (NAFOSTED) under grant number 107.04-2017.09.

5. References

[1] G. Robinson, J. B. C. Davies (1999) *Continuum robot – A state of art*. Proceedings of the IEEE International conference on robotics and automation Detroit Michigan, USA.

[2] M. W. Hannan, I. D. Walker (2003) Kinematics and the implementation of an Elephant's trunk manipulator and other continuum style robots. Journal of robotics, vol. 20, no. 2, pp. 45-63.

[3] T. Zheng, D. T. Branson, G. Emanuele and D. G. Caldwell (2011) *A 3D Dynamic Model for Continuum Robots Inspired by an Octopus Arm*. Proceedings of the IEEE International conference on robotics and automation, Shanghai, China.

[4] R, Kang, D. T. Branson, G. Emanuele, D. G. Caldwell (2012) *Dynamic modeling and control of an octopus inspired multiple continuum arm robot.* Computers and Mathematics with Applications, vol. 64, pp. 1004-1016.

[5] Matteo Cianchetti, M Calisti, L. Margheri, M. Kuba, C Laschi (2015) *Bioinspired locomotion and grasping in water: the soft eight-arm OCTOPUS robot*. Bioinspiration & Biomimetics, DOI: 10.1088/1748-3190/10/3/035003.

[6] L. Ming, M. Agheli, C. D. Onal (2014) Theoretical Modeling and Experimental Analysis of a Pressure-Operated Soft Robotic Snake. Soft robotics, vol. 1, no. 2, pp. 136-146.

[7] B. K. Jessica, D. C. Rucker (2015) *Continuum Robots for Medical Applications: A Survey*. Transactions on robotics, DOI: 10.1109/TRO.2015.2489500

[8] M. B. Wooten, I. D. Walker (2018) *Vine-Inspired Continuum Tendril Robots and Circumnutations*. Robotics, vol. 7, no. 58, pp. 2-16.

[9] Y. Azamat, K. Koichi, Y. Yoshiro (2019) *Design and Kinematics of Cable-Driven Continuum Robot Arm with Universal Joint Backbone*. Proceedings of the 2018 IEEE International conference on robotics and biomimetics, Kuala Lumpur, Malaysia.

[10] F. Renda, M Giorelli, M. Calisti, M Cianchetti, C. Laschi (2014) *Dynamic Model of a Multibending Soft Robot Arm Driven by Cables*. IEEE Trasactions on robotics, pp. 1-14.

[11] Y. Liu, J. Chen, J. Liu (2018) *Nonlinear mechanics of flexible cables in space robotic arms subject to complex physical environment*. Nonlinear dynamic.

[12] Y. Han, L. Zhou, W. Xu (2019) A comprehensive static model of cable-driven multi-section continuum robots considering friction effect. Mechanism and Machine Theory, vol. 135, pp. 130-149.

[13] Amouri, C. Mahfoudi, S. Djeffal (2019) *Kinematic and Dynamic Modeling and Simulation Analysis of a cable-driven continuum robot*. Computational Methods and Experimental Testing in Mechanical Engineering, pp. 27-37.

[14] D. C. Rucker, R. J. Webster (2011) *Statics and Dynamics of Continuum Robots with General Tendon Routing and External Loading*. Transactions on robotics, vol. 27, no. 6, pp. 1033-1044.

[15] S. R. William, P. B. Tzvi (2014) *Continuum Robot Dynamics Utilizing the Principle of Virtual Power*. Transactions on robotics, vol. 30, no. 1, pp. 275-287.

[16] L. Zheng, W. Liao, R. Hongliang, Y. Haoyong (2017) *Kinematic comparison of surgical tendon-driven manipulators and concentric tube manipulators*. Mechanism and Machine Theory, vol. 107, pp. 148-165.

[17] Mukherjee, A. Senpupta, S. Bhaumik (2018) *Kinematics and Teleoperation of Tendon Driven Continuum Robot*. International Conference on Robotics and Smart Manufacturing (RoSMa2018), vol. 138, pp. 879-886.

[18] D. C. Rucker, R. J. Webster (2011) *Statics and Dynamics of Continuum Robots with General Tendon Routing and External Loading*. Transactions on robotics, vol. 27, no. 6, pp. 1033-1044.

[19] B. Marshal, I. D. Walker (2004) *Novel continuum robots with variable-length sections*. IFAC 2004, Salemo, Italy.

[20] B. A. Jones, I. D. Walker (2006) *Kinematics for Multi-section Continuum Robots*. IEEE/ASME Transactions on mechatronics, vol. 22, no. 1, pp. 43-55.

[21] Amouri, C. Mahfoudi, A. Zaatri, h. Merabti (2014) *A New Approach to Solve Inverse Kinematics of a Planar Flexible Continuum Robot*. International Conference of Computational Methods in Sciences and Engineering 2014 (ICCMSE 2014), pp. 643-646.

[22] Amouri, C. Mahfoudi, A. Zaatri, L. Othman, R. Merzouki (2017) *A metaheuristic approach to solve inverse kinematics of continuum manipulators*. Journal of Systems and Control Engineering, DOI: 10.1177/0959651817700779.

[23] X. Dong, R. Mark, C. G. Salvandor, A. Dragos (2016) *A novel continuum robot using Twin-pivot compliant joints: design, modeling and validation*. Journal of mechanism and robotics, vol. 8, pp. 01-14.

[24] S. Geng, Y. Wang, C. Wang, R. Kang (2018) *A Space Tendon-Driven Continuum Robot*. Springer International Publishing AG, part of Springer Nature 2018, pp. 25–35.